JOURNAL OF AIRCRAFT
Vol. 43, No. 6, November–December 2006

Structural Ritz-Based Simple-Polynomial Nonlinear Equivalent Plate Approach: An Assessment

Luciano Demasi* and Eli Livne†
University of Washington, Seattle, Washington 98195-2400

DOI: 10.2514/1.17466

The linear equivalent plate approach developed and used for the aeroelastic optimization of composite wings at the conceptual design stage is a Ritz approach based on simple polynomial functions as generalized coordinates. Generalization to the case of geometrically nonlinear structural behavior is presented here in an effort to assess accuracy and performance of the method in the nonlinear static and linear dynamic cases. Using the von Kármán plate formulation for moderately large deformations, three-dimensional assemblies of thin-plate segments are modeled using a penalty function approach to impose boundary conditions and compatibility of motion between adjacent segments. Closed-form expressions for mass and stiffness terms (linear and nonlinear) make numerical integration unnecessary. Numerical results obtained by the present method for a variety of plate structures, in both static and dynamic cases, show good correlation with published results and results by other computer codes. Results by the present formulation are also compared with large-deformation results. Limits of applicability, in terms of the range of deformations still captured accurately by the equivalent plate method, are studied in all test cases.

Nomenclature

$\boldsymbol{A}$, $\boldsymbol{D}$	=	plate stiffness matrices
a	=	reference length (different for all cases)
E	=	elastic modulus
$\boldsymbol{F}^u$, $\boldsymbol{F}^v$, $\boldsymbol{F}^w$	=	vectors containing the Ritz functions used for the expansion of the displacements
h	=	thickness of the plate
$\boldsymbol{J}$	=	Jacobian matrix
$\boldsymbol{K}_{l_0 l_0}$, $\boldsymbol{K}_{l_1 l_1}$	=	linear stiffness matrices
$\boldsymbol{K}_{l_0 nl}$, $\boldsymbol{K}_{nll_0}$	=	nonlinear stiffness matrices with linear dependence on $\boldsymbol{q}_w$
$\boldsymbol{K}_{nlnl}$	=	nonlinear stiffness matrix with quadratic dependence on $\boldsymbol{q}_w$
k_x, k_y, k_z	=	stiffness of the springs used to impose boundary conditions
L_e	=	external work
$\boldsymbol{M}^1$, $\boldsymbol{M}^2$	=	contributions to the consistent mass matrix
N_u, N_v, N_w	=	number of Ritz functions used in the expansion of the displacements
$\bar{P}$	=	nondimensional external pressure
$\bar{\boldsymbol{Q}}$	=	elastic matrix
$\boldsymbol{q}$	=	generalized displacements
$\boldsymbol{q}_w$	=	generalized displacements (only the part related to the out-of-plane displacement)
q_0	=	pressure amplitude
S	=	surface
$\boldsymbol{T}$	=	traction force per unit area
t	=	time
U	=	potential energy
u, v, w	=	displacements in x, y, and z direction, respectively
$\bar{u}$, $\bar{v}$, $\bar{w}$	=	nondimensional displacements
$\ddot{\boldsymbol{u}}$, $\ddot{\boldsymbol{q}}$	=	physical and generalized acceleration vectors
V	=	volume
υ	=	Poisson's ratio
x, y, z	=	coordinate system (local for the wing segments, otherwise global)
γ_{zx}, γ_{zy}, ε_{zz}	=	out-of-plane strains
δ	=	variational operator
$\boldsymbol{\varepsilon}$	=	strain vector
$\boldsymbol{\varepsilon}_{l_0}$, $\boldsymbol{\varepsilon}_{l_1}$	=	vectors of the linear strains
$\boldsymbol{\varepsilon}_{nl}$	=	vector of the nonlinear strains
ε_{xx}, γ_{xy}, ε_{yy}	=	in-plane strains
ξ, η	=	natural coordinates
ρ	=	material density
$\boldsymbol{\sigma}$	=	stress vector
σ_{I}, σ_{II}	=	maximum and minimum principal stresses
σ_{xx}, τ_{xy}, σ_{yy}	=	in-plane stresses
ω	=	angular frequency

Subscripts

bot	=	referred to the bottom surface of the plate
max	=	referred to the maximum value
top	=	referred to the top surface of the plate
u	=	related to the displacement u
v	=	related to the displacement v
w	=	related to the displacement w
$,x$	=	first derivative with respect to x
$,xx$	=	second derivative with respect to x
$,xy$	=	second derivative with respect to x and y
$,y$	=	first derivative with respect to y
$,yy$	=	second derivative with respect to y
0	=	referred to the middle plane of the plate

Superscripts

T	=	transpose
u	=	related to the displacement u
v	=	related to the displacement v
w	=	related to the displacement w

Introduction

IN the case of linear structural/aeroelastic analysis, equivalent plate models based on Ritz series solutions using simple polynomials were found to be fast and adequately accurate for design

Presented as Paper 2093 at the 46th AIAA/ASME/ASCE/AHS/ASC Structures, Structural Dynamics, and Materials Conference, Austin, Texas, 18–21 April 2005; received 1 May 2005; revision received 15 February 2006; accepted for publication 16 March 2006.

*Postdoctoral Research Associate, Department of Aeronautics and Astronautics, Box 352400. Member AIAA.

†Professor, Department of Aeronautics and Astronautics, Box 352400. Associate Fellow AIAA.

optimization of aircraft in the very early design stages. Among the advantages such models [1–6] offer are the following:

1) Ease of model generation, modeling wings of general planforms as assemblages of large p-type trapezoidal structural elements.

2) Analytical closed-form expressions for all mass and stiffness matrix elements, making numerical integration unnecessary.

3) Continuous, closed-form, dependency of deformations (and stresses) over large wing segments, simplifying the structural mesh to aerodynamic mesh interpolation problem on spatial location considerably.

4) Low-order system's equations, leading to low-order matrices.

The introduction of structural nonlinearity makes the generation of structural models and structural analysis simulations more complex and computationally intensive [7]. It was only natural to hope that the extension of the equivalent plate methodology to the case of the nonlinear structural dynamics will yield numerically efficient adequately accurate structural simulation capability for conceptual-stage aeroelastic design optimization of structurally nonlinear lifting surface configurations.

The goal of the proposed paper is to describe the development of such a nonlinear equivalent plate capability and the assessment of its accuracy and numerical performance.

Two variants of the structural plate approach will be described: a MATLAB-based version [7] based on the series summation approach of the classical linear equivalent plate technique, and a FORTRAN-based version based on closed-form formulas obtained symbolically.

This paper will present the mathematical theory behind both equivalent plate approaches and discuss numerical implementation issues. It will then continue to assess accuracy and computational performance of the various methods using some simple plate models as well as more challenging plate assemblies and prototype joined-wing configurations. Both linear and nonlinear results will be presented and compared with linear and fully nonlinear NASTRAN results to highlight differences in performance among the methods in the linear and nonlinear cases. The paper will conclude with lessons to date regarding the usefulness of equivalent plate wing models in the structurally nonlinear aeroelasticity case.

Description of the Structural Model

The mathematical model is created by assembling nonlinear plate elements (denoted as wing segments). Boundary conditions and compatibility constraints used to connect different segments to one another are imposed by a penalty function method [8]. The physical meaning of the weights used for the penalty terms is that of physical stiff springs that force points to move together. This discretization is shown in Fig. 1. Wing segments are modeled as solid thin plates, with planar cross sections remaining planar and staying perpendicular to the plate's reference surface. Equivalent plate modeling of real flight vehicle wings must include transverse shear effects [2]. However, based on past experience [6], plate models based on classical plate theory (CPT) were used in the present investigation to focus on the comparison between linear and nonlinear structural behavior. They were found to portray the same behavior in terms of accuracy and convergence with simple-polynomial Ritz function as plate models based on first-order shear deformation plate theory (FSDPT). Because correlation with finite element codes is used to assess the accuracy of the polynomial-based Ritz method, this removes one potential source of difference among different capabilities (that is, the way transverse shear effects are modeled). Simple thin-plate aeroelastic wind tunnel models used for experimental studies of wings and joined wings provide additional motivation for the CPT modeling used here.

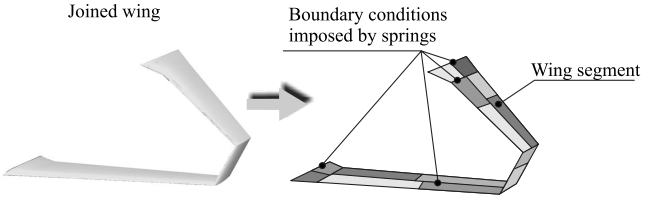

Fig. 1 Joined-wing discretization using trapezoidal wing segments.

Strain-displacement assumptions of the von Kármán plate theory for moderately large displacements are expressed in

$$\varepsilon_{xx} = u_{,x} + \tfrac{1}{2}w_{,x}^2 \qquad \varepsilon_{yy} = v_{,y} + \tfrac{1}{2}w_{,y}^2$$
$$\gamma_{xy} = (u_{,y} + v_{,x}) + w_{,x}w_{,y} \tag{1}$$

In accordance with classical plate theory, it is also assumed that each layer (lamina) of the plate is in-plane strain:

$$\gamma_{zx} = \gamma_{zy} = \varepsilon_{zz} = 0 \tag{2}$$

For the displacement field, CPT is based on

$$u(x, y, z, t) = u_0(x, y, t) - zw_{0_{,x}}(x, y, t)$$
$$v(x, y, z, t) = v_0(x, y, t) - zw_{0_{,y}}(x, y, t) \tag{3}$$
$$w(x, y, z, t) = w_0(x, y, t)$$

Multiplication of the equations of equilibrium by virtual displacements and integration over the plate's volume lead to the virtual work principle in the form

$$\int_V \sigma_{ij}\delta\varepsilon_{ij}\,\mathrm{d}v + \int_V \rho\ddot{u}_i\delta u_i\,\mathrm{d}v = \int_S T_i\delta u_i\,\mathrm{d}s \tag{4}$$

where T_i is the traction force per unit of area. For the layer-by-layer plane stress case, the last equation can be written as

$$\int_V (\sigma_{xx}\delta\varepsilon_{xx} + \sigma_{yy}\delta\varepsilon_{yy} + \tau_{xy}\delta\gamma_{xy})\,\mathrm{d}v + \int_V \rho(\ddot{u}\delta u + \ddot{v}\delta v + \ddot{w}\delta w)\,\mathrm{d}v$$
$$= \int_S (T_x\delta u + T_y\delta v + T_z\delta w)\,\mathrm{d}S \tag{5}$$

Hooke's law is

$$\boldsymbol{\sigma} = \bar{\boldsymbol{Q}}\boldsymbol{\varepsilon} \tag{6}$$

where

$$\boldsymbol{\sigma} = \begin{bmatrix}\sigma_{xx} & \sigma_{yy} & \tau_{xy}\end{bmatrix}^T \qquad \boldsymbol{\varepsilon} = \begin{bmatrix}\varepsilon_{xx} & \varepsilon_{yy} & \gamma_{xy}\end{bmatrix}^T \tag{7}$$

$$\bar{\boldsymbol{Q}} = \begin{bmatrix}\bar{Q}_{11} & \bar{Q}_{12} & \bar{Q}_{16} \\ \bar{Q}_{12} & \bar{Q}_{22} & \bar{Q}_{26} \\ \bar{Q}_{16} & \bar{Q}_{26} & \bar{Q}_{66}\end{bmatrix} \tag{8}$$

Notice that $\bar{Q}$ is layer dependent. Equation (5) becomes

$$\int_V \delta\boldsymbol{\varepsilon}^T\bar{\mathrm{Q}}\boldsymbol{\varepsilon}\,\mathrm{d}v + \int_V \rho\delta\boldsymbol{u}^T\ddot{\boldsymbol{u}}\,\mathrm{d}v = \int_S \delta\boldsymbol{u}^T\boldsymbol{T}\,\mathrm{d}s \tag{9}$$

The strains can be written as [Eqs. (1) and (3)]

$$\boldsymbol{\varepsilon} = \boldsymbol{\varepsilon}_{l_0} - z\boldsymbol{\varepsilon}_{l_1} + \boldsymbol{\varepsilon}_{nl} \tag{10}$$

where

$$\boldsymbol{\varepsilon}_{l_0} = \begin{bmatrix} u_{0_{,x}} \\ v_{0_{,y}} \\ u_{0_{,y}} + v_{0_{,x}}\end{bmatrix} \qquad \boldsymbol{\varepsilon}_{l_1} = \begin{bmatrix} w_{0_{,xx}} \\ w_{0_{,yy}} \\ 2w_{0_{,xy}}\end{bmatrix} \qquad \boldsymbol{\varepsilon}_{nl} = \begin{bmatrix} \tfrac{1}{2}w_{0_{,x}}^2 \\ \tfrac{1}{2}w_{0_{,y}}^2 \\ w_{0_{,x}}w_{0_{,y}}\end{bmatrix} \tag{11}$$

Carrying out the volume integration, first with respect to z and then with respect to x and y and using the matrices

$$\boldsymbol{A} = \int_z \bar{\mathrm{Q}}\,\mathrm{d}z \qquad \boldsymbol{D} = \int_z z^2\bar{\mathrm{Q}}\,\mathrm{d}z \tag{12}$$

one can write, in the case of symmetric layups (the reference plane x, y is the middle plane of the plate),

$$\int_V \delta\boldsymbol{\varepsilon}^T \bar{\mathbf{Q}}\boldsymbol{\varepsilon}\,\mathrm{d}v = \int_{x,y} \delta\boldsymbol{\varepsilon}_{l_0}^T \boldsymbol{A}\boldsymbol{\varepsilon}_{l_0}\mathrm{d}x\mathrm{d}y + \int_{x,y} \delta\boldsymbol{\varepsilon}_{l_0}^T \boldsymbol{A}\boldsymbol{\varepsilon}_{nl}\mathrm{d}x\mathrm{d}y + \int_{x,y} \delta\boldsymbol{\varepsilon}_{l_1}^T \boldsymbol{D}\boldsymbol{\varepsilon}_{l_1}\,\mathrm{d}x\,\mathrm{d}y + \int_{x,y} \delta\boldsymbol{\varepsilon}_{nl}^T \boldsymbol{A}\boldsymbol{\varepsilon}_{l_0}\,\mathrm{d}x\,\mathrm{d}y + \int_{x,y} \delta\boldsymbol{\varepsilon}_{nl}^T \boldsymbol{A}\boldsymbol{\varepsilon}_{nl}\,\mathrm{d}x\,\mathrm{d}y \tag{13}$$

The present formulation is valid for symmetric layups of composite laminates. However, all the results shown in this paper have been obtained considering isotropic materials.

Ritz Discretization

Solutions for the displacement field are sought by using a set of Ritz functions as generalized coordinates:

$$\begin{aligned} u_0(x,y,t) &= F_1^u(x,y)q_{u_1}(t) + F_2^u(x,y)q_{u_2}(t) + \ldots + F_{N_u}^u(x,y)q_{u_{N_u}}(t) \\ v_0(x,y,t) &= F_1^v(x,y)q_{v_1}(t) + F_2^v(x,y)q_{v_2}(t) + \ldots + F_{N_v}^v(x,y)q_{v_{N_v}}(t) \\ w_0(x,y,t) &= F_1^w(x,y)q_{w_1}(t) + F_2^w(x,y)q_{w_2}(t) + \ldots + F_{N_w}^w(x,y)q_{w_{N_w}}(t) \end{aligned} \tag{14}$$

Here [1–7] polynomials of the type $x^s y^r$ are used as Ritz functions to create complete polynomials.

It is well known that simple polynomials lead to ill conditioning [9–11] when used as Ritz functions, as terms with high powers r and s are present alongside low-order terms. However, simple polynomials lead to a greatly simplified problem formulation, and if a configuration is divided into relatively small segments where low-order polynomials are used, ill conditioning is not a problem.

Using a more compact notation, the displacement field [Eq. (14)] is expressed as

$$\begin{bmatrix} u_0 \\ v_0 \\ w_0 \end{bmatrix} = \begin{bmatrix} \boldsymbol{F}^{uT} & \boldsymbol{0}^{vT} & \boldsymbol{0}^{wT} \\ \boldsymbol{0}^{uT} & \boldsymbol{F}^{vT} & \boldsymbol{0}^{wT} \\ \boldsymbol{0}^{uT} & \boldsymbol{0}^{vT} & \boldsymbol{F}^{wT} \end{bmatrix} \cdot \begin{bmatrix} \boldsymbol{q}_u \\ \boldsymbol{q}_v \\ \boldsymbol{q}_w \end{bmatrix} \tag{15}$$

Substitution into Eqs. (11) and (13) now leads to

$$\int_V \delta\boldsymbol{\varepsilon}^T \bar{\mathbf{Q}}\boldsymbol{\varepsilon}\,\mathrm{d}v = \delta\boldsymbol{q}^T\boldsymbol{K}_{l_0l_0}\boldsymbol{q} + \delta\boldsymbol{q}^T\boldsymbol{K}_{l_0nl}\boldsymbol{q} + \delta\boldsymbol{q}^T\boldsymbol{K}_{l_1l_1}\boldsymbol{q} + \delta\boldsymbol{q}^T\boldsymbol{K}_{nll_0}\boldsymbol{q} + \delta\boldsymbol{q}^T\boldsymbol{K}_{nlnl}\boldsymbol{q} \tag{16}$$

where $\boldsymbol{K}_{l_0l_0}$ and $\boldsymbol{K}_{l_1l_1}$ are the *linear* stiffness matrices and $\boldsymbol{K}_{l_0nl}$, $\boldsymbol{K}_{nll_0}$, and $\boldsymbol{K}_{nlnl}$ are the *nonlinear* stiffness matrices. Because of the simple-polynomial nature of the Ritz function used, all volume integrals over trapezoidal plate segments can be carried out analytically *without any need for numerical integration*. For a *symmetric* layup and *uniform density*, the inertial terms are

$$\int_V \rho\delta\boldsymbol{u}^T\ddot{\boldsymbol{u}}\,\mathrm{d}v = \delta\boldsymbol{q}^T\boldsymbol{M}^1\ddot{\boldsymbol{q}} + \delta\boldsymbol{q}^T\boldsymbol{M}^2\ddot{\boldsymbol{q}} \tag{17}$$

The virtual work equation [Eqs. (13) and (16)] now takes the form

$$\delta\boldsymbol{q}^T[\boldsymbol{K}_{l_0l_0} + \boldsymbol{K}_{l_0nl} + \boldsymbol{K}_{l_1l_1} + \boldsymbol{K}_{nll_0} + \boldsymbol{K}_{nlnl}]\boldsymbol{q} + \delta\boldsymbol{q}^T[\boldsymbol{M}^1 + \boldsymbol{M}^2]\ddot{\boldsymbol{q}} = \delta L_e \tag{18}$$

where δL_e is the external virtual work. The explicit expression for the mass matrices is

$$\boldsymbol{M}^1 = \rho h \begin{bmatrix} \int_{x,y} \boldsymbol{F}^u\boldsymbol{F}^{uT}\,\mathrm{d}x\,\mathrm{d}y & \boldsymbol{0}^u\boldsymbol{0}^{vT} & \boldsymbol{0}^u\boldsymbol{0}^{wT} \\ \boldsymbol{0}^v\boldsymbol{0}^{uT} & \int_{x,y} \boldsymbol{F}^v\boldsymbol{F}^{vT}\,\mathrm{d}x\,\mathrm{d}y & \boldsymbol{0}^v\boldsymbol{0}^{wT} \\ \boldsymbol{0}^w\boldsymbol{0}^{uT} & \boldsymbol{0}^w\boldsymbol{0}^{vT} & \int_{x,y} \boldsymbol{F}^w\boldsymbol{F}^{wT}\,\mathrm{d}x\,\mathrm{d}y \end{bmatrix} \tag{19}$$

$$\boldsymbol{M}^2 = \frac{\rho h^3}{12} \begin{bmatrix} \boldsymbol{0}^u\boldsymbol{0}^{uT} & \boldsymbol{0}^u\boldsymbol{0}^{vT} & \boldsymbol{0}^u\boldsymbol{0}^{wT} \\ \boldsymbol{0}^v\boldsymbol{0}^{uT} & \boldsymbol{0}^v\boldsymbol{0}^{vT} & \boldsymbol{0}^v\boldsymbol{0}^{wT} \\ \boldsymbol{0}^w\boldsymbol{0}^{uT} & \boldsymbol{0}^w\boldsymbol{0}^{vT} & \int_{x,y} \boldsymbol{F}_{,x}^w\boldsymbol{F}_{,x}^{wT}\,\mathrm{d}x\,\mathrm{d}y + \int_{x,y} \boldsymbol{F}_{,y}^w\boldsymbol{F}_{,y}^{wT}\,\mathrm{d}x\,\mathrm{d}y \end{bmatrix} \tag{20}$$

Imposition of the Boundary Conditions

Stiffness and mass matrices are calculated for each wing segment separately in local coordinate axes for the segment. In assembling a configuration from segments, boundary conditions have to be imposed as well as compatibility conditions between segments. Displacements and/or rotations between two adjacent wing segments must be the same depending on the actual way in which they are connected. Displacements and/or rotations have to be zero at points or along lines attached to the ground.

One of the essential features of the finite element method is that generalized displacements are actual physical displacements and rotations of element nodes. By adding to the proper locations in the global stiffness and mass matrices stiffness and mass contributions of elements that share the same nodes, compatibility of motion is guaranteed at those nodes. But compatibility of motion is not guaranteed along common edges of elements, and what convergence characteristics "compatible" or "incompatible" various plate elements have is one of the most challenging problems of plate and shell finite elements.

When generalized coordinates in the form of global Ritz functions over elements are used, constraint equations or constraint terms must be used to impose compatibility of displacement and rotation between elements. A penalty function technique [8] is used here to impose compatibility along sides of adjacent plate elements.

Any order of Ritz functions can be used over a plate segment, whereas element-to-element attachments are enforced by lines of stiff springs.

To do that it is sufficient to place a sufficient number of springs along the edge between two adjacent wing segments. To impose compatibility of the rotations between two wing segments, if only translational springs are used, it is sufficient to place translational springs in different positions across the thickness.

Consider a simple case where two points, 1_A on wing segment A and 1_B on wing segment B, have to be linked by springs (Fig. 2). The procedure is based on the following steps:

1) The displacement field at point 1_A in the *local coordinate system* on the wing segment A is considered.

2) The *global coordinates* of the same point are determined by multiplying by a geometric transformation matrix from local A axes to global axes.

3) The same procedure is applied to point 1_B on the wing segment B.

4) The *potential energy* of springs linking the x–y–z motions of points 1_A and 1_B is written as

$$U = \frac{1}{2}\left[\begin{bmatrix} u_{1_A} \\ v_{1_A} \\ w_{1_A} \end{bmatrix}_g - \begin{bmatrix} u_{1_B} \\ v_{1_B} \\ w_{1_B} \end{bmatrix}_g\right]^T \begin{bmatrix} k_x^1 & 0 & 0 \\ 0 & k_y^1 & 0 \\ 0 & 0 & k_z^1 \end{bmatrix} \left[\begin{bmatrix} u_{1_A} \\ v_{1_A} \\ w_{1_A} \end{bmatrix}_g - \begin{bmatrix} u_{1_B} \\ v_{1_B} \\ w_{1_B} \end{bmatrix}_g\right] \tag{21}$$

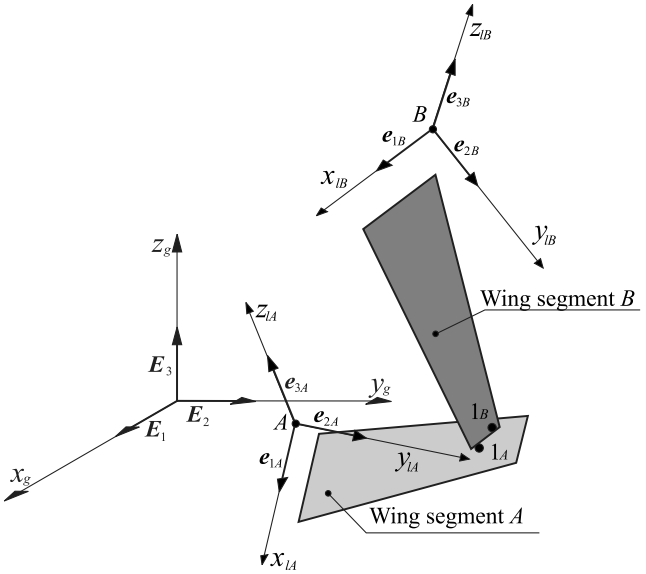

Fig. 2 Imposition of boundary conditions by springs.

The subscripts g in the previous equation indicate that the displacements have to be referred to the *global coordinate system*.

5) Substitution of the Ritz function series approximations for the displacements of 1_A and 1_B in axes A and B, respectively [Eqs. (14) and (15)], and using the subscripts A and B for the generalized coordinates on the wing segments A and B, the potential energy can be rewritten as

$$U = \tfrac{1}{2}\left[\boldsymbol{q}_A^T\left(\boldsymbol{K}_{AA}^{s1}\right)\boldsymbol{q}_A + \boldsymbol{q}_A^T\left(\boldsymbol{K}_{AB}^{s1}\right)\boldsymbol{q}_B + \boldsymbol{q}_B^T\left(\boldsymbol{K}_{BA}^{s1}\right)\boldsymbol{q}_A + \boldsymbol{q}_B^T\left(\boldsymbol{K}_{BB}^{s1}\right)\boldsymbol{q}_B\right] \tag{22}$$

The quantities $\boldsymbol{K}_{AA}^{s1}$, $\boldsymbol{K}_{AB}^{s1}$, $\boldsymbol{K}_{BA}^{s1}$, $\boldsymbol{K}_{BB}^{s1}$ are the stiffness matrices that have to be added to the total stiffness matrix in locations corresponding to generalized coordinates $\boldsymbol{q}_A$ and $\boldsymbol{q}_B$ (Fig. 3). The superscript S_i in Fig. 3 denotes a family of springs connecting segments A and C to the ground and to segment B in regions 1, 2, 3, 4.

Analytical Integration

An advantage of the usage of the Ritz functions in the form $x^s y^r$ is that it is possible to use *analytical* integration to calculate the integrals over a trapezoidal domain (the middle surface of the wing segment).

Consider a wing segment in which two edges are parallel to the local x axis (it is possible to divide the wing into segments with this characteristic without losing generality), as shown in Fig. 4. The front and rear (aft) lines depend on the coordinates of the vertices of the trapezoid and are defined by the equations:

$$x_F(y) = F_1 y + F_2 \qquad x_A(y) = A_1 y + A_2 \tag{23}$$

where

$$F_1 = \frac{x_{FR} - x_{FL}}{y_R - y_L}; \qquad F_2 = \frac{x_{FL}y_R - x_{FR}y_L}{y_R - y_L} \qquad A_1 = \frac{x_{AR} - x_{AL}}{y_R - y_L}$$
$$A_2 = \frac{x_{AL}y_R - x_{AR}y_L}{y_R - y_L} \tag{24}$$

The integral of any simple-polynomial term with powers r and s over the wing is of the type

$$I_{\mathrm{TR}}(r,s) = \int_{y=y_L}^{y=y_R} y^r \int_{x=x_F(y)}^{x=x_A(y)} x^s \,\mathrm{d}x\,\mathrm{d}y = \frac{1}{s+1}\int_{y=y_L}^{y=y_R} y^r[x_A(y)^{s+1} - x_F(y)^{s+1}]\,\mathrm{d}y = \frac{1}{s+1}\int_{y=y_L}^{y=y_R} y^r(A_1 y + A_2)^{s+1}\,\mathrm{d}y - \frac{1}{s+1}\int_{y=y_L}^{y=y_R} y^r(F_1 y + F_2)^{s+1}\,\mathrm{d}y = \frac{1}{S}\int_{y=y_L}^{y=y_R} y^R(A_1 y + A_2)^S\,\mathrm{d}y - \frac{1}{S}\int_{y=y_L}^{y=y_R} y^R(F_1 y + F_2)^S\,\mathrm{d}y \tag{25}$$

The last two integrals can be calculated by using recursive formulas:

$$\int y^R(A_1 y + A_2)^S\,\mathrm{d}y = \frac{y^{R+1}(A_1 y + A_2)^S}{R+S+1} + \frac{SA_2}{R+S+1}\int y^R(A_1 y + A_2)^{S-1}\,\mathrm{d}y \tag{26}$$

$$\int y^R(F_1 y + F_2)^S\,\mathrm{d}y = \frac{y^{R+1}(F_1 y + F_2)^S}{R+S+1} + \frac{SF_2}{R+S+1}\int y^R(F_1 y + F_2)^{S-1}\,\mathrm{d}y \tag{27}$$

A table of integrals of simple-polynomial functions of increasing order is prepared once for each trapezoidal segment at the start of a simulation run up to the highest order needed. Integrals of $x^s y^r$ over the trapezoid are then taken from such tables during the stiffness and mass matrix assembly process. Different runs using different order polynomials for the displacement fields can then be carried out using the same table of integrals prepared initially. This approach has been used in the MATLAB-based version of the present structural plate model. However, it is possible to predetermine the Ritz functions that are used and, therefore, all integrals can be calculated *once and a priori* using a symbolic commercial code such as MATHEMATICA. Using this procedure, all mass, linear and nonlinear stiffness matrices can be calculated in closed form reducing the number of operations that have to be performed at each iteration in the nonlinear solution process. MATHEMATICA-derived closed-form matrices have been used in the FORTRAN-based version of the code. Note that although terms of the linear stiffness matrix are independent of generalized displacements, $\boldsymbol{q}$, the nonlinear parts of the stiffness matrix do depend on $\boldsymbol{q}$ (more precisely, the nonlinear matrices depend on $\boldsymbol{q}_w$ only. If the tangent matrix is calculated, it depends also on the other components of the vector $\boldsymbol{q}$), and closed-form expressions for these terms contain dependency on the generalized displacements. These generalized displacements vary under load.

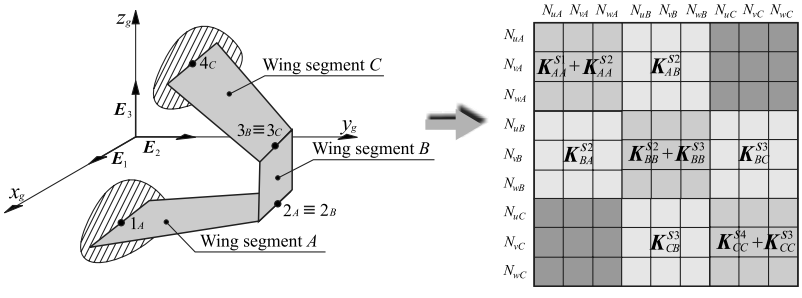

Fig. 3 Example of imposition of boundary conditions by springs.

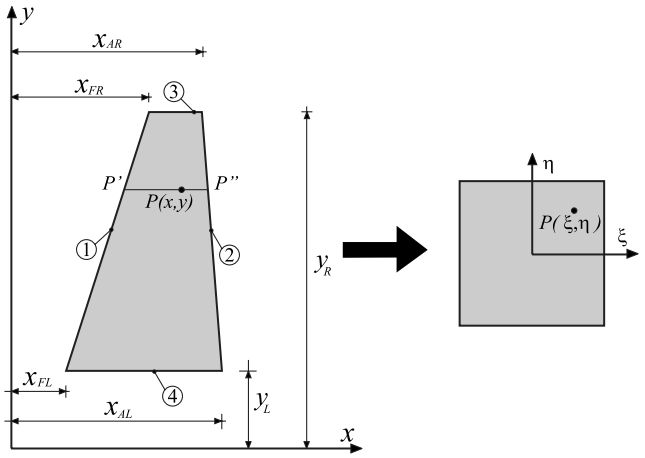

Fig. 4 Geometry and notation of a trapezoidal wing segment.

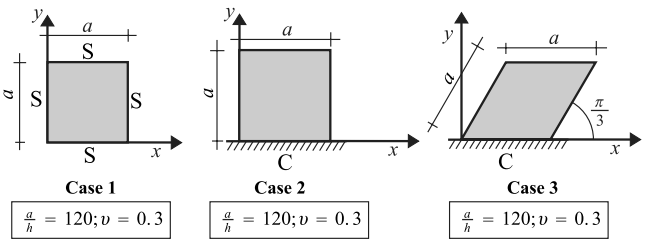

Fig. 5 Cases 1, 2, and 3: geometry and notations.

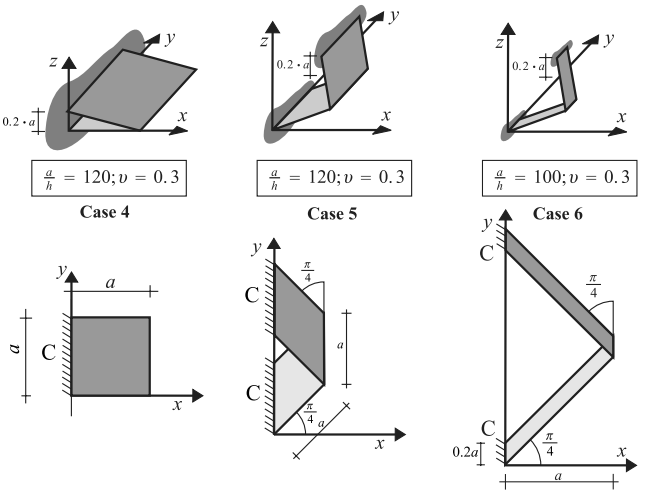

Fig. 6 Cases 4, 5, and 6: geometry and notations.

Solution of the Nonlinear System

Several methods are presented in literature for the integration and solution of fully nonlinear structural analysis problems [12–19]. In the formulation used here for the moderately small deformations of plates, the *Newton–Raphson method* and the *direct method* have been adopted. In the Newton–Raphson method, only the tangent matrix has been used, whereas in the direct method only the secant matrix [20] has been used. Although the linear part of the stiffness matrix is calculated once, the nonlinear parts, which depend on the motion $\boldsymbol{q}$, have to be repetitively calculated during simulation (in the FORTRAN-based version of the code the matrices are obtained in closed form using MATHEMATICA).

Selected Test Problems

A number of test cases were selected for evaluation of the nonlinear structural wing plate analysis described here. Results of the present capability were compared with reported results from the literature and with MSC-NASTRAN solutions. In all MSC-NASTRAN cases plate elements (CQUAD4 or CTRIA3) were used. The following cases were analyzed (see Figs. 5 and 6):

Case 1: square plate simply supported along its perimeter.

Case 1 is selected because it is a standard test case for any nonlinear plate simulation. The focus of the development here, though, is wings and not panels.

Case 2: square cantilevered wing.
Case 3: swept cantilevered wing.
Case 4: joined wing (first model).
Case 5: joined wing (second model).
Case 6: joined wing (third model).

In all cases, the load was represented by an uniform pressure q_0 with direction $+z$.

Results

Results of displacement predictions, natural frequencies (for the linear case), and stresses obtained by the Ritz-based plate approach (denoted RVKPF) by finite elements (NASTRAN) are discussed in the following paragraphs.

In all cases the quantities (stresses and/or displacements) are calculated in different locations. The point in which the quantities are calculated is denoted with the letter *P*.

Case 1: Square Plate Simply Supported Along Its Perimeter

The following NASTRAN meshes have been used:
Mesh 1: CQUAD4 4 × 4;
Mesh 2: CQUAD4 10 × 10;
Mesh 3: CQUAD4 20 × 20;
Mesh 4: CTRIA3 4 × 4;
Mesh 5: CTRIA3 10 × 10;
Mesh 6: CTRIA3 20 × 20.

Natural frequencies for the simply supported square plate are listed in Table 1, and show less than 1% error in the predicted 4th frequency with 8th order Ritz polynomials compared with the converged NASTRAN result. The results obtained by using mesh 1 and mesh 4 were not converged and, therefore, they are not reported in Table 1. Normalized vertical displacement at the center of the plate is shown versus the normalized load in Fig. 7, and the correlation between the RVKPF approach and the finite element (FE) approach is excellent

Table 1 Case 1: frequency parameter; comparison RVKPF vs NASTRAN

Frequency parameter	$\omega_1\sqrt{a^4\rho/(Eh^2)}$	$\omega_2\sqrt{a^4\rho/(Eh^2)}$	$\omega_3\sqrt{a^4\rho/(Eh^2)}$	$\omega_4\sqrt{a^4\rho/(Eh^2)}$
ANALYTICAL[a]	5.973	14.933	14.933	23.893
NASTRAN (mesh 2)	5.887	14.645	14.645	22.841
NASTRAN (mesh 3)	5.937	14.824	14.824	23.508
NASTRAN (mesh 5)	5.938	14.902	14.902	23.779
NASTRAN (mesh 6)	5.951	14.900	14.900	23.800
RVKPF (order 6)	5.975	17.849	17.849	28.004
RVKPF (order 7)	5.975	14.980	14.982	28.005
RVKPF (order 8)	5.973	14.981	14.981	24.026
RVKPF (order 9)	5.973	14.927	14.931	24.014

[a]The analytical value of the frequency parameter has been calculated using the formula for simply supported square plates, $\sqrt{\pi^4/[12(1-\upsilon^2)]}(n^2+m^2)$.

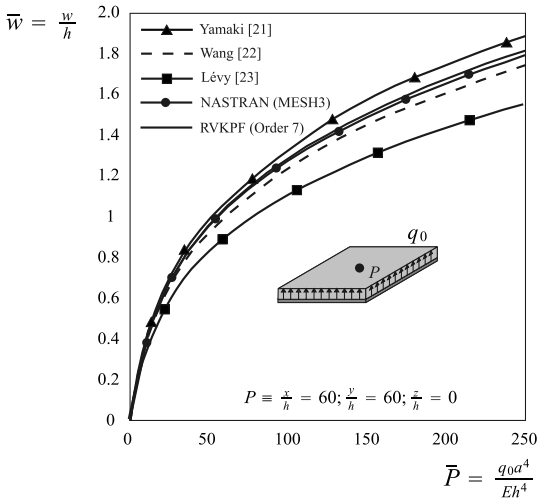

Fig. 7 Case 1: nondimensional maximum deflection.

throughout the range of loading considered. Comparison with other results available in the literature [21–23] is also made.

Case 2: Square Cantilevered Wing

The same NASTRAN meshes as in the case 1 have been used. Normalized natural frequencies of the cantilevered square plate are shown in Table 2. With 7th-order Ritz polynomials the RVKPF approach leads to frequency values for the 4th natural frequency that are about 1.5% different than corresponding FE frequencies. In-plane (Fig. 8) and out-of-plane (Fig. 9) displacements and principal stresses (Fig. 10) at selected points on the plate show good correlation between Ritz and FE predictions. Note the smaller loading range covered in this case compared with the simply supported case, the larger out-of-plane displacement (in terms of h), and the nonlinear behavior of the in-plane displacement that starts at relatively low loading values.

Case 3: Swept Cantilevered Wing

The meshes are the same as the meshes used in cases 1 and 2. Normalized natural frequencies for the swept cantilevered plate are listed in Table 3, with about 2% difference between 7th order Ritz plate and FE prediction for the 4th natural frequency. Excellent correlation between RVKPF based on 7th order polynomials and the FE result is evident in Fig. 11 for the out-of-plane displacement. In-plane displacements obtained by the Ritz-based plate method are less accurate compared with the FE results, but they capture the nonlinear behavior very well (Fig. 12). As to principal stresses on the top surface of the plate, the smaller principal stress (not shown here) is captured well. In the case of the larger principal stress (Fig. 13), large errors begin to accumulate even at relatively low loading and reach about 20% at the highest loading tested. Note that stresses in Fig. 13 are calculated at a point not too far away from the rear point on the root of the wing, a region known for its steep stress gradients in the case of swept-back wings. In this area FE stress results become quite sensitive to the FE mesh used.

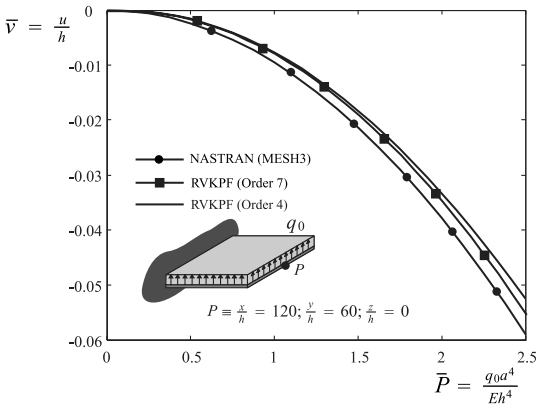

Fig. 8 Case 2: nondimensional displacement $\bar{u}$.

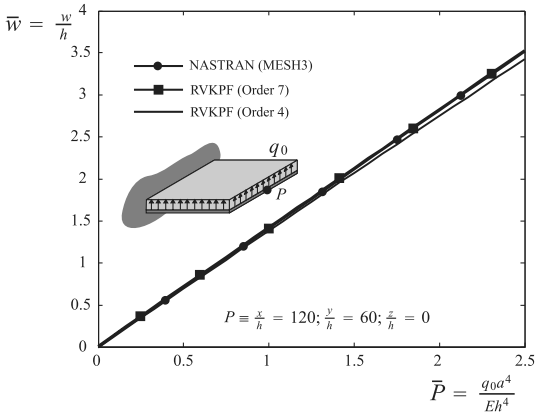

Fig. 9 Case 2: nondimensional displacement $\bar{w}$.

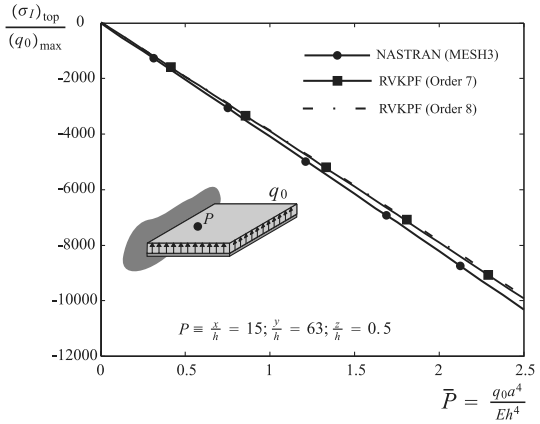

Fig. 10 Case 2: nondimensional maximum principal stress.

Table 2 Case 2: frequency parameter; comparison RVKPF vs NASTRAN

Frequency parameter	$\omega_1\sqrt{a^4\rho/(Eh^2)}$	$\omega_2\sqrt{a^4\rho/(Eh^2)}$	$\omega_3\sqrt{a^4\rho/(Eh^2)}$	$\omega_4\sqrt{a^4\rho/(Eh^2)}$
NASTRAN (mesh 2)	1.046	2.533	6.321	7.957
NASTRAN (mesh 3)	1.049	2.560	6.408	8.151
NASTRAN (mesh 5)	1.047	2.544	6.339	8.009
NASTRAN (mesh 6)	1.049	2.563	6.412	8.167
RVKPF (order 6)	1.057	2.584	6.454	8.409
RVKPF (order 7)	1.055	2.578	6.450	8.291
RVKPF (order 8)	1.053	2.578	6.449	8.233
RVKPF (order 9)	1.052	2.577	6.449	8.230

Table 3 Case 3: frequency parameter; comparison RVKPF vs NASTRAN

Frequency parameter	$\omega_1\sqrt{a^4\rho/(Eh^2)}$	$\omega_2\sqrt{a^4\rho/(Eh^2)}$	$\omega_3\sqrt{a^4\rho/(Eh^2)}$	$\omega_4\sqrt{a^4\rho/(Eh^2)}$
NASTRAN (mesh 2)	1.182	2.810	7.499	7.618
NASTRAN (mesh 3)	1.187	2.833	7.606	7.778
NASTRAN (mesh 5)	1.187	2.829	7.564	7.730
NASTRAN (mesh 6)	1.188	2.841	7.632	7.810
RVKPF (order 6)	1.198	2.945	8.048	8.195
RVKPF (order 7)	1.194	2.909	7.853	7.974
RVKPF (order 8)	1.192	2.882	7.741	7.887
RVKPF (order 9)	1.191	2.871	7.708	7.863

Case 4: Joined Wing (First Model)

The following meshes have been used:

Mesh 7: CQUAD4 10×10 for each wing;

Mesh 8: CQUAD4 20×20 for each wing.

Table 4 shows normalized natural frequencies for the simple joined-wing (JW) model of test case 4. A difference of about 5% is obtained between the Ritz-based plate approach and the NASTRAN-FE result with just two large plate segments (an upper one and a lower one) with 8th order polynomial displacements on each. The joined-wing case is challenging because of its 3-D geometry, and the fact that under upwards pressure loads the upper wing is under compression.

Displacement (Figs. 14 and 15) and stress accuracy (Figs. 16 and 17) of the nonlinear Ritz-based plate method was excellent up to normalized loads of about 30, and was quite good up to the full loads tested. The Ritz-plate results in Figs. 16 and 17 were obtained using 8 large plate segments (4 on the top and 4 on the bottom plates) with 8th order polynomial Ritz functions on each segment.

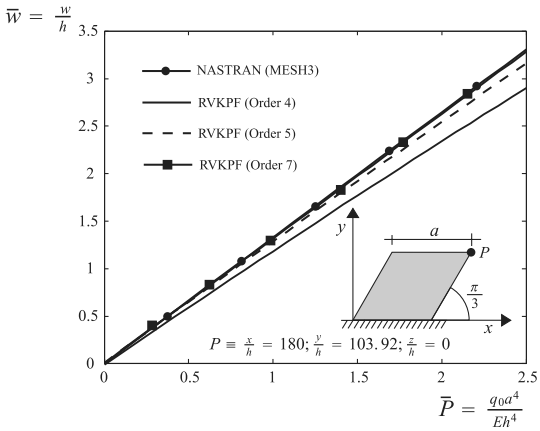

Fig. 11 Case 3: nondimensional displacement $\bar{w}$.

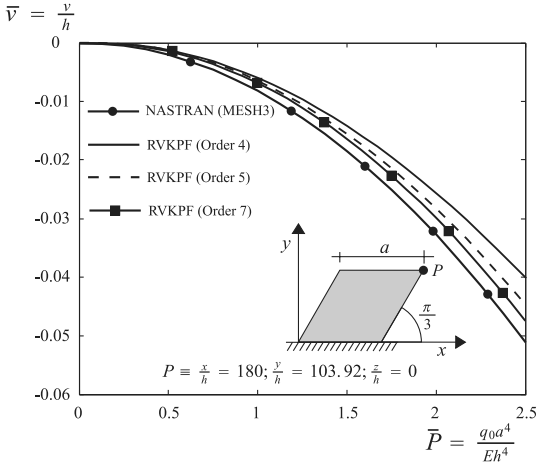

Fig. 12 Case 3: nondimensional displacement $\bar{v}$.

Case 5: Joined Wing (Second Model)

The following mesh has been used in the NASTRAN computations:

Mesh 8: CQUAD4 20×20 for each wing.

When the JW configuration is swept so that the upper wing is swept forward and the lower wing is swept back the case becomes even more challenging. Now steep stress gradients appear near the rear corner root point of the lower wing and the front corner root point of the upper wing. The simple-polynomial Ritz functions have to capture displacement behavior over distorted wing segments in space. As Figs. 18–20 show, displacements are captured well by the Ritz-based plate method up to a normalized load of about 25. Out-of-plane displacements are predicted well beyond that load, but the authors found that the in-plane displacements in a particular location of the wing (where a local effect is important, see Fig. 21) become less accurate as the load increases (though their trends are captured well). Wing twist results are shown in Fig. 22, whereas principal stresses are compared in Figs. 23 and 24. Note the excellent correlation of principal stresses along leading edge of upper wing. As the root is approached, the well known stress rise is evident.

If the deformed shape is analyzed (see Fig. 21) it appears clear that the local effect on the swept-forward wing (the upper wing) becomes increasingly important when $\bar{P}$ increases. To capture well this local effect several wing segments are required. The authors found that the approximation is acceptable when the upper wing is divided into nine wing segments and the lower wing is divided into four wing segments.

Case 6: Joined Wing (Third Model)

The following mesh has been used in the NASTRAN model:

Mesh 9: CQUAD4 50×10 for each wing.

Finally, the 3rd joined-wing model, made of two higher aspect ratio segments compared with the JW of the previous case, is used to assess the accuracy of the Ritz-based plate method. Results are shown in Figs. 25–29. The RVKPF approach captures displacements, angle of attack (twist), and stresses well. Deterioration of accuracy of the Ritz-plate stress prediction is observed in Fig. 29 above a normalized load of 1.

In all nonlinear cases studied computational efficiency of the NASTRAN-FE solution was at least an order of magnitude higher

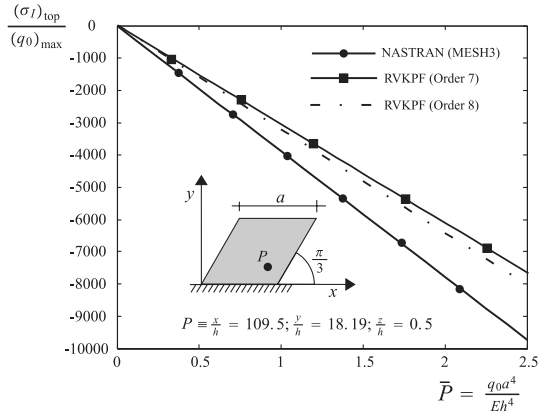

Fig. 13 Case 3: nondimensional maximum principal stress.

Table 4 Case 4: frequency parameter; comparison RVKPF vs NASTRAN

Frequency parameter	$\omega_1\sqrt{a^4\rho/(Eh^2)}$	$\omega_2\sqrt{a^4\rho/(Eh^2)}$	$\omega_3\sqrt{a^4\rho/(Eh^2)}$	$\omega_4\sqrt{a^4\rho/(Eh^2)}$
NASTRAN (mesh 7)	4.466	5.947	6.584	7.727
NASTRAN (mesh 8)	4.463	6.011	6.579	7.814
RVKPF (order 8)	4.481	6.088	6.846	8.228
RVKPF (order 9)	4.479	6.085	6.854	8.175

than that of any of the Ritz-plate approaches tested (the MATLAB-based version of the code was compiled using the internal MATLAB C/C++ compiler MCC). Although the Ritz-based plate approach leads to a smaller number of degrees of freedom in the resulting model, the sparseness of the FE matrices allows solutions of the matrix equations to be fast and efficient. This becomes even more pronounced in the case of nonlinear structural analysis, where nonlinear stiffness equations have to be solved repetitively.

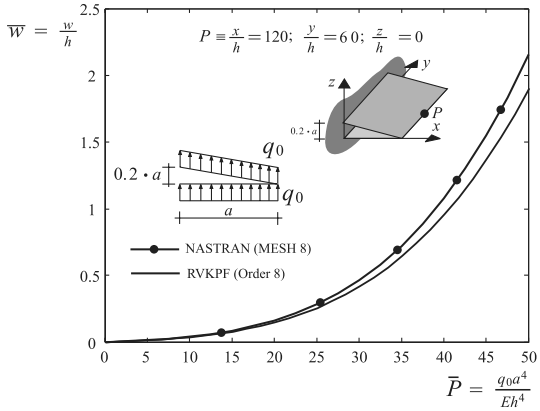

Fig. 14 Case 4: nondimensional displacement $\bar{w}$; RVKPF vs NASTRAN.

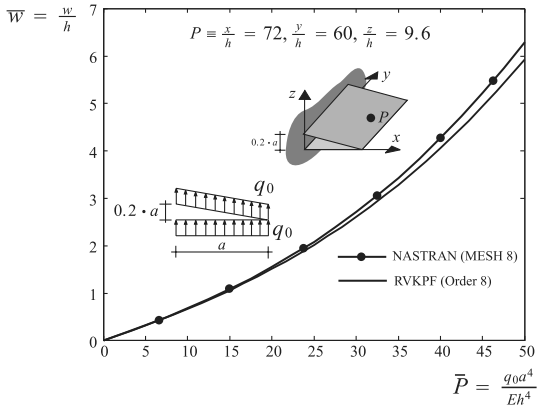

Fig. 15 Case 4: nondimensional displacement $\bar{w}$; RVKPF vs NASTRAN.

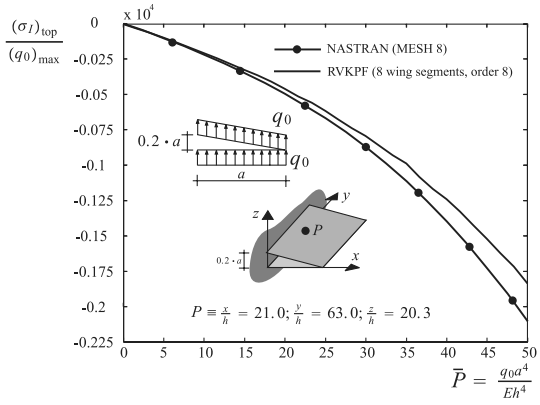

Fig. 16 Case 4: nondimensional maximum principal stress.

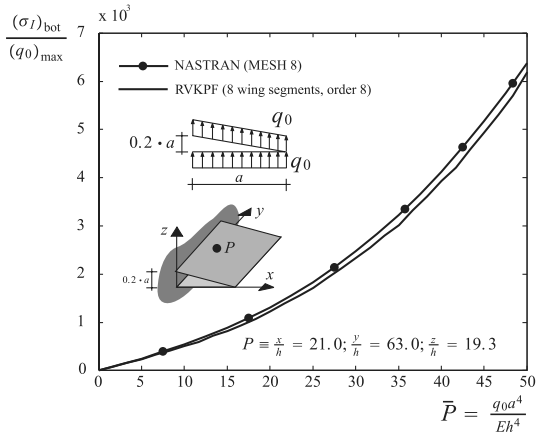

Fig. 17 Case 4: nondimensional maximum principal stress.

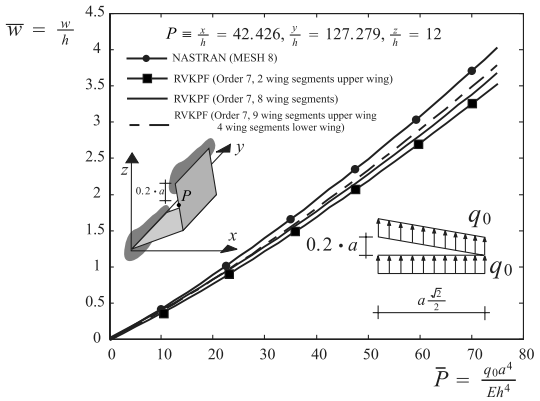

Fig. 18 Case 5: nondimensional displacement $\bar{w}$.

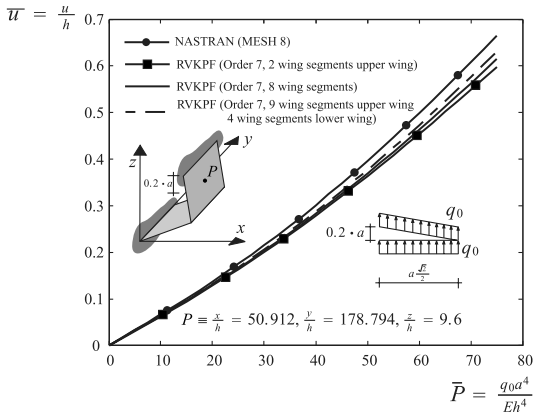

Fig. 19 Case 5: nondimensional displacement $\bar{u}$.

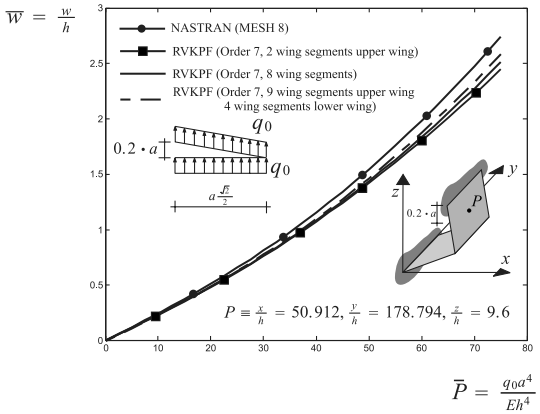

Fig. 20 Case 5: nondimensional displacement $\bar{w}$.

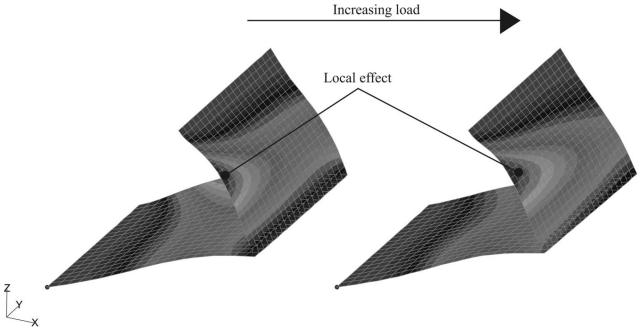

Fig. 21 Case 5: deformed surface (NASTRAN).

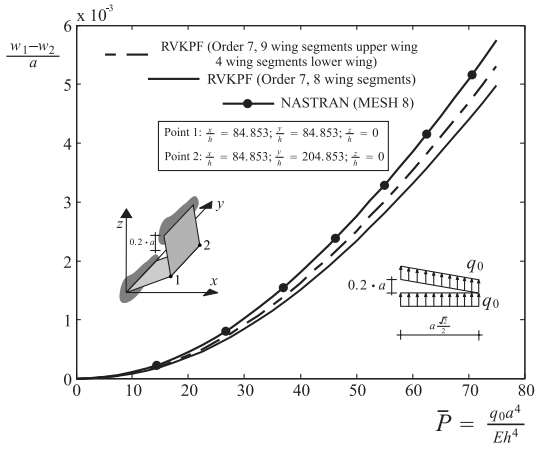

Fig. 22 Case 5: wing twist.

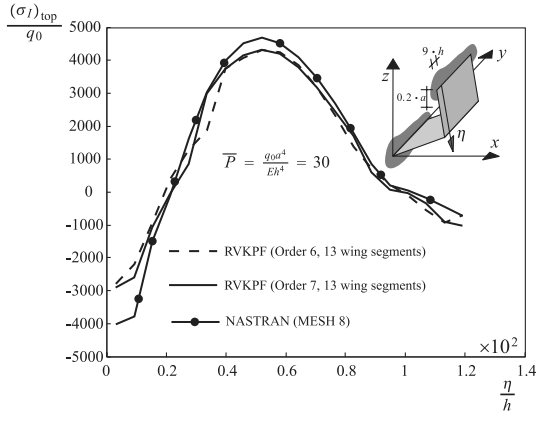

Fig. 23 Case 5: nondimensional maximum principal stress.

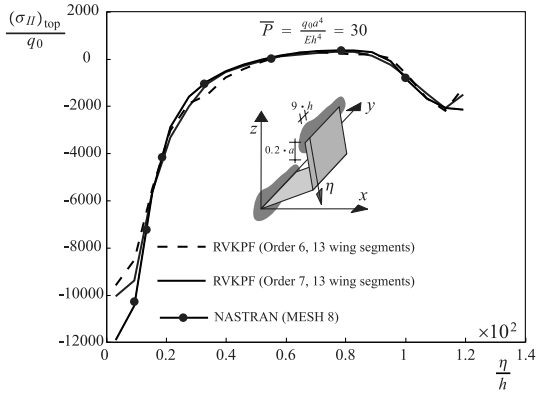

Fig. 24 Case 5: nondimensional minimum principal stress.

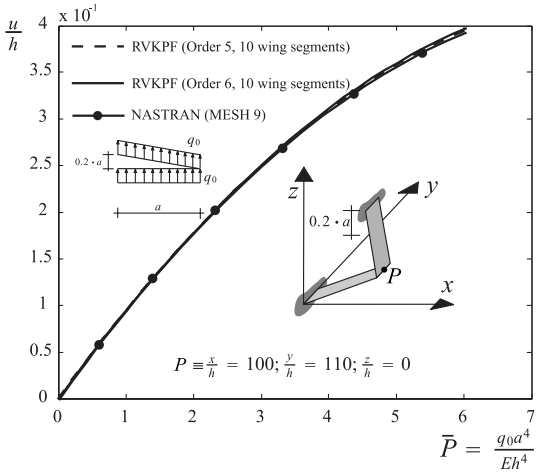

Fig. 25 Case 6: nondimensional tip displacement u/h.

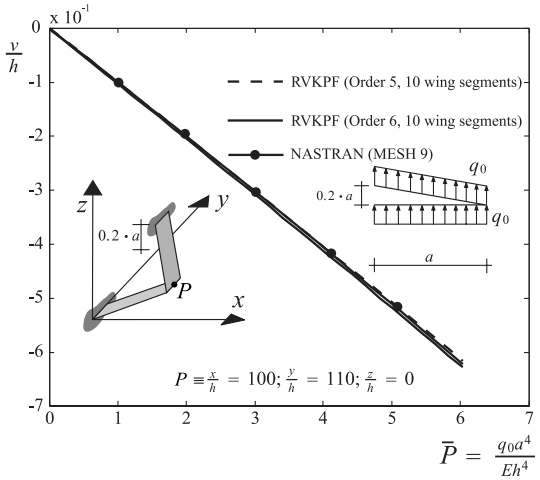

Fig. 26 Case 6: nondimensional tip displacement v/h.

The calculation of nonlinear stiffness terms with the Ritz-plate approach is done in closed form, but it involves time consuming high-order do-loops, and that, when high-order Ritz polynomials are used, contributes significantly to the increase in computing time, compared with the FE method, which uses lower order polynomials. Because of this slow computation and the large number of plates needed to achieve the convergence (for complex configurations), the FE approach is recommended for the nonlinear structural and aeroelastic studies of joined-wing configurations. The authors

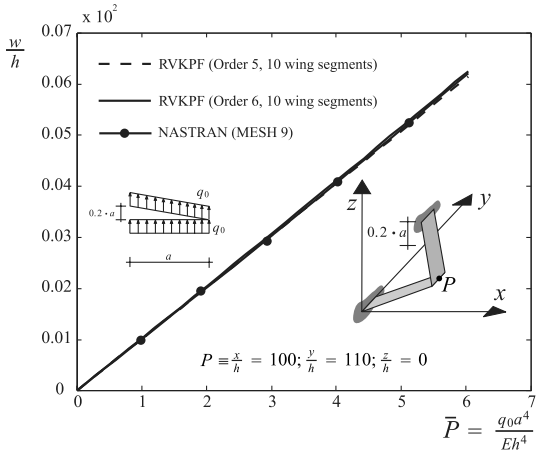

Fig. 27 Case 6: nondimensional displacement w/h.

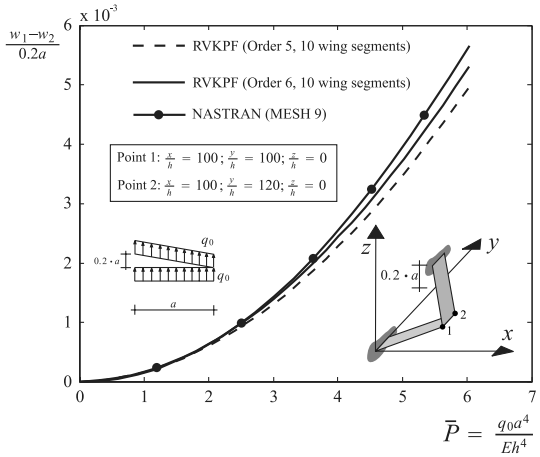

Fig. 28 Case 6: wing twist.

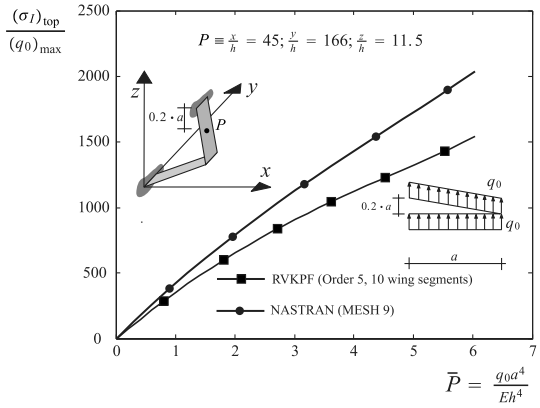

Fig. 29 Case 6: nondimensional maximum principal stress.

studied joined wings [24] using the updated Lagrangian formulation of Levy and Gal [25,26]) and they found a better correlation with NASTRAN and much better computational speed compared with their Ritz-plate capabilities described here.

It can be concluded that despite the attractiveness of the simple-polynomial Ritz approach and its simple (theoretically if only a few large wing segments are used) structural-aerodynamic mesh interaction, the Ritz-based plate approach is not recommended for the study of nonplanar wings (such as joined wings). Recent results [27] for the case of nonlinear aeroelasticity of a delta wing show better correlation with experimental results when general nonlinear finite elements were used compared with a plate approach based on von Kármán's assumptions and theory. When nonlinear effects become important on cantilevered and 3-D wing assemblies, out-of-plane displacements can be larger than a few times the thickness of the plates. It is the panel flutter case, where panel boundaries are constrained and out-of-plane displacements are small, that nonlinearity begins at relatively low loads and can be well captured by the Ritz-based plate theory [28,29]. Additional figures showing predicted behavior of in-plane displacements, minimal principal stresses, and other functions of plate and joined-wing structural response can be found in [30].

Conclusions

The von Kármán Ritz-plate formulation is very effective when the geometry of the structure is relatively simple (square, rectangular, swept but not by too much) and the resulting motion is not too large relative to the thickness of the plates. In such conditions, a single wing segment can describe well the displacement field and stresses at all points of the plate. Linear, nonlinear, static, and dynamic cases can be effectively studied.

When the geometry/load configuration is complex (3-D, swept and distorted wing segments, in-plane compression or tension in segments), a single wing segment is not enough to obtain a good accuracy. Expecting displacement gradients in areas of abrupt geometric changes, or segment-to-segment joints more wing segments have to be used and the computation can be considerably slow compared with NASTRAN-FE capability. Because of this slow computation and the large number of plates needed, the FE approach is recommended for the nonlinear structural and aeroelastic studies of joined-wing configurations.

One of the questions to be addressed when extending the Ritz-based plate approach to the nonlinear case was sensitivity of boundary conditions constraints to the spring values used. The authors performed several convergence tests (not shown here for brevity) and demonstrated that a good choice for the spring stiffness is a value of the order of the Young Modulus E (for isotropic materials, but similar conclusions can be found for an orthotropic material). The results were found to be insensitive to spring values around this order of magnitude.

The compatibility of the rotations (between wing segments or the boundary) can be imposed using translational springs disposed across the thickness. The authors did an extensive study on the effect (not reported here for brevity) of the distance between the springs. No significant difference has been found.

Once the convergence has been achieved, the displacements and their spatial derivatives are well approximated. Therefore, the stresses can be calculated without problems even where the springs are located.

If the aspect ratio of the wing segments is quite small (for example, if the ratio is 0.2), an ill conditioning appears at low order of the polynomials used in the Ritz functions. This problem can partially be avoided by using more wing segments. However, the best approach would be the use of *orthogonal* polynomials (e.g., Legendre polynomials), but this last method has not been used here.

It can be concluded that despite the attractiveness of the simple-polynomial Ritz approach and its simple (theoretically if only a few large wing segments are used) structural-aerodynamic mesh interaction, the Ritz-based plate approach is not recommended for the study of geometrically nonlinear nonplanar wings (such as joined wings).

Appendix A: Details About the Nonlinear Matrices

In this Appendix one term of the $\boldsymbol{K}_{nlnl}$ matrix is expressly shown. That matrix can be written as

$$\boldsymbol{K}_{nlnl} = \boldsymbol{K}^1_{nlnl} + \boldsymbol{K}^2_{nlnl} + \boldsymbol{K}^3_{nlnl} + \boldsymbol{K}^4_{nlnl} + \boldsymbol{K}^5_{nlnl} + \boldsymbol{K}^6_{nlnl} + \boldsymbol{K}^7_{nlnl} + \boldsymbol{K}^8_{nlnl} + \boldsymbol{K}^9_{nlnl} \tag{A1}$$

The term $\boldsymbol{K}^9_{nlnl}$ is

$$\boldsymbol{K}^{9}_{nlnl} = \frac{A_{66}}{2}\begin{bmatrix} \mathbf{0}^{u}\mathbf{0}^{uT} & \mathbf{0}^{u}\mathbf{0}^{vT} & \mathbf{0}^{u}\mathbf{0}^{wT} \\ \mathbf{0}^{v}\mathbf{0}^{uT} & \mathbf{0}^{v}\mathbf{0}^{vT} & \mathbf{0}^{v}\mathbf{0}^{wT} \\ \mathbf{0}^{w}\mathbf{0}^{uT} & \mathbf{0}^{w}\mathbf{0}^{vT} & \int_{x,y}\left[\boldsymbol{F}^{w}_{,y}\boldsymbol{F}^{wT}_{,x} + \boldsymbol{F}^{w}_{,x}\boldsymbol{F}^{wT}_{,y}\right]\boldsymbol{q}_{w}\boldsymbol{q}^{T}_{w}\left[\boldsymbol{F}^{w}_{,x}\boldsymbol{F}^{wT}_{,y} + \boldsymbol{F}^{w}_{,y}\boldsymbol{F}^{wT}_{,x}\right]\mathrm{d}x\,\mathrm{d}y \end{bmatrix} \tag{A2}$$

Appendix B: Transformation of the Integrals to Perform Their Analytical Computation

The integrals that compare in the nonlinear stiffness matrices have to be transformed to perform the analytical calculation. This operation is required if the table of integrals calculated once is used. To illustrate the method, consider one of the integrals in the first term $\boldsymbol{K}^{1}_{nlnl}$:

$$\int_{x,y} \boldsymbol{F}^{w}_{,x}\boldsymbol{F}^{wT}_{,x}\boldsymbol{q}_{w}\boldsymbol{q}^{T}_{w}\boldsymbol{F}^{w}_{,x}\boldsymbol{F}^{wT}_{,x}\,\mathrm{d}x\,\mathrm{d}y \tag{B1}$$

It is easy to see that the terms $\boldsymbol{F}^{wT}_{,x}\boldsymbol{q}_{w}, \boldsymbol{q}^{T}_{w}\boldsymbol{F}^{w}_{,x}$ are *scalar* quantities. For this reason, they can be written as

$$\boldsymbol{F}^{wT}_{,x}\boldsymbol{q}_{w} = \boldsymbol{q}^{T}_{w}\boldsymbol{F}^{w}_{,x} \qquad \boldsymbol{q}^{Tw}\boldsymbol{F}^{w}_{,x} = \boldsymbol{F}^{wT}_{,x}\boldsymbol{q}_{w} \tag{B2}$$

By using these expressions, the integrals become

$$\begin{aligned} &\int_{x,y} \boldsymbol{F}^{w}_{,x}\boldsymbol{F}^{wT}_{,x}\boldsymbol{q}_{w}\boldsymbol{q}^{T}_{w}\boldsymbol{F}^{w}_{,x}\boldsymbol{F}^{wT}_{,x}\mathrm{d}x\mathrm{d}y \\ &= q_{wk_w}q_{wl_w}\int_{x,y} F^{w}_{,xk_w}F^{w}_{,xi_w}F^{w}_{,xj_w}F^{w}_{,xl_w}\,\mathrm{d}x\,\mathrm{d}y \\ &\qquad k_w, l_w, i_w, j_w = 1, \ldots, N_w \end{aligned} \tag{B3}$$

This expression is useful because in the integrals only Ritz functions of the type $x^s y^r$ appear and it is possible to use the analytical integration as seen above.

Appendix C: Numerical Integration

Even though area integrals in the Ritz-based simple-polynomial method can be obtained analytically, it was found that numerical integration led to much shorter computing times. The Gauss rule to integrate the functions over the wing area can be used. Therefore, a transformation (between physical coordinates and natural coordinates) is required. The equations of lines 1 and 2 (see Fig. 4) are

$$\frac{y - y_L}{y_R - y_L} = \frac{x - x_{FL}}{x_{FR} - x_{FL}} \qquad \frac{y - y_L}{y_R - y_L} = \frac{x - x_{AL}}{x_{AR} - x_{AL}} \tag{C1}$$

It can be observed that lines 3 and 4 are *parallel* to the x axis, and so *for this particular case*, y is a function only of η:

$$\frac{\eta + 1}{y - y_L} = \frac{2}{y_R - y_L} \Rightarrow y = \frac{\eta + 1}{2}(y_R - y_L) + y_L = y(\eta) \tag{C2}$$

Lines 1 and 2 *are not parallel* to the y axis, therefore, a *nonlinear* relation between x and ξ, η has to be found. Using Fig. 4:

$$\frac{\xi + 1}{x_P - x_{P'}} = \frac{2}{x_{P''} - x_{P'}} \tag{C3}$$

And from Eq. (C1):

$$\begin{aligned} x_{P'} &= \frac{y - y_L}{y_R - y_L}(x_{FR} - x_{FL}) + x_{FL} \\ x_{P''} &= \frac{y - y_L}{y_R - y_L}(x_{AR} - x_{AL}) + x_{AL} \end{aligned} \tag{C4}$$

substituting these last relations into Eq. (C3) and using Eq. (C2):

$$\begin{aligned} x = \tfrac{1}{4}[&\xi[(x_{AL} - x_{FL}) + (x_{AR} - x_{FR})] + \eta[(x_{AR} - x_{FL}) \\ &- (x_{AL} - x_{FR})] + \xi\eta[(x_{AR} - x_{FR}) - (x_{AL} - x_{FL})] \\ &+ x_{FL} + x_{FR} + x_{AR} + x_{AL}] = x(\xi, \eta) \end{aligned} \tag{C5}$$

This expression and Eq. (C2) can be simplified by introducing the quantities

$$\begin{aligned} X_1 &= \tfrac{1}{4}[(x_{AL} - x_{FL}) + (x_{AR} - x_{FR})] \\ X_2 &= \tfrac{1}{4}[(x_{AR} - x_{FL}) - (x_{AL} - x_{FR})] \\ X_3 &= \tfrac{1}{4}[(x_{AR} - x_{FR}) - (x_{AL} - x_{FL})] \\ X_4 &= \tfrac{1}{4}[x_{FL} + x_{FR} + x_{AR} + x_{AL}] \qquad Y_1 = \frac{y_R - y_L}{2} \\ Y_2 &= \frac{y_R + y_L}{2} \end{aligned} \tag{C6}$$

Finally, the relations are

$$y = Y_1\eta + Y_2 \qquad x = X_1\xi + X_2\eta + X_3\xi\eta + X_4 \tag{C7}$$

The inverse of the previous expression is

$$\xi = \frac{x - X_2[(y - Y_2)/Y_1] - X_4}{X_1 + X_3[(y - Y_2)/Y_1]} \qquad \eta = \frac{y - Y_2}{Y_1} \tag{C8}$$

To use the Gauss rule, the Jacobian matrix of the geometrical transformation shown in Fig. 4 is needed:

$$\boldsymbol{J} = \begin{bmatrix} \frac{\partial x}{\partial \xi} & \frac{\partial y}{\partial \xi} \\ \frac{\partial x}{\partial \eta} & \frac{\partial y}{\partial \eta} \end{bmatrix} \tag{C9}$$

And using Eq. (C7), the Jacobian matrix becomes

$$\boldsymbol{J} = \begin{bmatrix} X_1 + X_3\eta & 0 \\ X_2 + X_3\xi & Y_1 \end{bmatrix} \tag{C10}$$

The inverse of Jacobian matrix can easily be written as

$$\boldsymbol{J}^{-1} = \begin{bmatrix} \frac{1}{X_1 + X_3\eta} & 0 \\ -\frac{X_2 + X_3\xi}{(X_1 + X_3\eta)Y_1} & \frac{1}{Y_1} \end{bmatrix} \tag{C11}$$

Recalling the definition of Jacobian, the relation with the derivative operators is

$$\begin{bmatrix} \frac{\partial}{\partial \xi} \\ \frac{\partial}{\partial \eta} \end{bmatrix} = \begin{bmatrix} \frac{\partial x}{\partial \xi} & \frac{\partial y}{\partial \xi} \\ \frac{\partial x}{\partial \eta} & \frac{\partial y}{\partial \eta} \end{bmatrix} \cdot \begin{bmatrix} \frac{\partial}{\partial x} \\ \frac{\partial}{\partial y} \end{bmatrix} = \boldsymbol{J}\begin{bmatrix} \frac{\partial}{\partial x} \\ \frac{\partial}{\partial y} \end{bmatrix} \tag{C12}$$

In the considered case, the transformation is always possible. Because of that, the inverse of the previous relation can be written as

$$\begin{bmatrix} \frac{\partial}{\partial x} \\ \frac{\partial}{\partial y} \end{bmatrix} = \begin{bmatrix} \frac{\partial \xi}{\partial x} & \frac{\partial \eta}{\partial x} \\ \frac{\partial \xi}{\partial y} & \frac{\partial \eta}{\partial y} \end{bmatrix} \cdot \begin{bmatrix} \frac{\partial}{\partial \xi} \\ \frac{\partial}{\partial \eta} \end{bmatrix} = \boldsymbol{J}^{-1}\begin{bmatrix} \frac{\partial}{\partial \xi} \\ \frac{\partial}{\partial \eta} \end{bmatrix} \tag{C13}$$

The determinant of the Jacobian matrix is

$$\det \boldsymbol{J} = J_{11}J_{22} - J_{12}J_{21} = \frac{\partial x}{\partial \xi}\frac{\partial y}{\partial \eta} - \frac{\partial y}{\partial \xi}\frac{\partial x}{\partial \eta} \tag{C14}$$

And using relation (C10):

$$\det \boldsymbol{J} = (X_1 + X_3\eta)Y_1 \tag{C15}$$

Next focus is on the application of the numerical integration. For example, consider the matrix

$$\boldsymbol{K}^2_{l_0 l_0} = A_{12}\begin{bmatrix} \mathbf{0}^u\mathbf{0}^{uT} & \int_{x,y} \boldsymbol{F}^u_{,x}\boldsymbol{F}^{vT}_{,y}\,\mathrm{d}x\,\mathrm{d}y & \mathbf{0}^u\mathbf{0}^{wT} \\ \mathbf{0}^v\mathbf{0}^{uT} & \mathbf{0}^v\mathbf{0}^{vT} & \mathbf{0}^v\mathbf{0}^{wT} \\ \mathbf{0}^w\mathbf{0}^{uT} & \mathbf{0}^w\mathbf{0}^{vT} & \mathbf{0}^w\mathbf{0}^{wT} \end{bmatrix} \tag{C16}$$

The nonzero term is

$$\int_{x,y} \boldsymbol{F}^u_{,x}\boldsymbol{F}^{vT}_{,y}\mathrm{d}x\mathrm{d}y = \int_{x,y} F^u_{i,x}F^v_{j,x}\mathrm{d}x\mathrm{d}y = \int_{x,y} \frac{\partial F^u_i}{\partial x}\frac{\partial F^v_j}{\partial y}\,\mathrm{d}x\,\mathrm{d}y = I_{ij}$$
$$i = 1,\ldots,N_u, \qquad j = 1,\ldots,N_v \tag{C17}$$

By using Eq. (C13), the partial derivatives can be written as

$$\frac{\partial F^u_i(x,y)}{\partial x} = J^{-1}_{11}\frac{\partial F^u_i(\xi,\eta)}{\partial \xi} + J^{-1}_{12}\frac{\partial F^u_i(\xi,\eta)}{\partial \eta} = \frac{1}{X_1 + X_3\eta}\frac{\partial F^u_i(\xi,\eta)}{\partial \xi}$$
$$\frac{\partial F^v_j(x,y)}{\partial y} = J^{-1}_{21}\frac{\partial F^u_j(\xi,\eta)}{\partial \xi} + J^{-1}_{22}\frac{\partial F^u_j(\xi,\eta)}{\partial \eta}$$
$$= -\frac{X_2 + X_3\xi}{(X_1 + X_3\eta)Y_1}\frac{\partial F^u_j(\xi,\eta)}{\partial \xi} + \frac{1}{Y_1}\frac{\partial F^u_j(\xi,\eta)}{\partial \eta} \tag{C18}$$

With this relation, and recalling the geometrical transformation, the integral becomes

$$I_{ij} = \int_{\xi,\eta} \frac{1}{X_1 + X_3\eta}\frac{\partial F^u_i(\xi,\eta)}{\partial \xi}\left(-\frac{X_2 + X_3\xi}{(X_1 + X_3\eta)Y_1}\frac{\partial F^u_j(\xi,\eta)}{\partial \xi} + \frac{1}{Y_1}\frac{\partial F^u_j(\xi,\eta)}{\partial \eta}\right)\det \boldsymbol{J} \tag{C19}$$

Appendix D: Transformation of the Integrals to Perform Their Numerical Computation

The integrals that compare in the nonlinear stiffness matrices have to be transformed to perform the numerical calculation and improve the speed of the code. It is possible to avoid the four loops in the nonlinear matrices. To illustrate the method, consider one of the integrals in the first term $\boldsymbol{K}^1_{nlnl}$. In Appendix B it has been proven that

$$\int_{x,y} \boldsymbol{F}^w_{,x}\boldsymbol{F}^{wT}_{,x}\boldsymbol{q}_w\boldsymbol{q}^T_w\boldsymbol{F}^w_{,x}\boldsymbol{F}^{wT}_{,x}\mathrm{d}x\mathrm{d}y$$
$$= q_{wk_w}q_{wl_w}\int_{x,y} F^w_{,xk_w}F^w_{,xi_w}F^w_{,xj_w}F^w_{,xl_w}\,\mathrm{d}x\,\mathrm{d}y \tag{D1}$$
$$k_w, l_w, i_w, j_w = 1,\ldots,N_w$$

which allows one to easily write the derivatives with respect to the generalized coordinates and, therefore, to write the tangent matrix. This approach has been followed by the authors, but it is a computationally expensive method. The reason is that a cycle with four loops has to be performed (see the integral in which 4 indices appear). It is possible to avoid this problem by using only the secant matrix [20] in the nonlinear iterative solution. The convergence ratio is well known to be worse than the Newton–Raphson approach, but the secant matrix can be modified to have a cycle with only two loops (and, thus, much faster). This operation is performed here by using the relation

$$w_{0,x} = \boldsymbol{q}^T_w\boldsymbol{F}^w_{,x} = \boldsymbol{F}^{wT}_{,x}\boldsymbol{q}_w \tag{D2}$$

Substituting inside the equation representing the integral [Eq. (D1)]:

$$\int_{x,y} \boldsymbol{F}^w_{,x}\boldsymbol{F}^{wT}_{,x}\boldsymbol{q}_w\boldsymbol{q}^T_w\boldsymbol{F}^w_{,x}\boldsymbol{F}^{wT}_{,x}\,\mathrm{d}x\,\mathrm{d}y = \int_{x,y} w^2_{0,x}\boldsymbol{F}^w_{,x}\boldsymbol{F}^{wT}_{,x}\,\mathrm{d}x\,\mathrm{d}y \tag{D3}$$

The other integrals can be treated similarly and they can be numerically calculated as explained above in Appendix C.

References

[1] Giles, G. L., "Equivalent Plate Analysis of Aircraft Wing Box Structures with General Planform Geometry," *Journal of Aircraft*, Vol. 23, No. 11, 1986, pp. 859–864.

[2] Livne, E., "Equivalent Plate Structural Modeling for Wing Shape Optimization Including Transverse Shear," *AIAA Journal*, Vol. 32, No. 6, 1994, pp. 1278–1288.

[3] Giles, G. L., "Equivalent Plate Modeling for Conceptual Design of Aircraft Wing Structures," AIAA Paper 95-3945, Sept. 1995.

[4] Livne, E., Sels, R. A., and Bhatia, K. G., "Lessons from Application of Equivalent Plate Structural Modeling to an HASCT Wing," *Journal of Aircraft*, Vol. 31, No. 4, 1994, pp. 953–960.

[5] Livne, E., and Navarro, I., "Nonlinear Equivalent Plate Modeling of Wing-Box Structures," *Journal of Aircraft*, Vol. 36, No. 5, Sept.–Oct. 1999.

[6] Navarro, I., "Nonlinear Equivalent Plate Modeling of Wing Structures," M.S. Thesis, Department of Aeronautics, Univ. of Washington, Seattle, WA, 1997.

[7] Demasi, L., and Livne, E., "A Plate Structural Modeling Capability for the Nonlinear Aeroelastic Analysis of Joined-Wing Confgurations," *Proceeding of the XVII National Italian Conference AIDAA*, 2003.

[8] Felippa, C. A., "Error Analysis of Penalty Function Techniques for Constraint Definition in Linear Algebraic System," *International Journal for Numerical Methods in Engineering*, Vol. 11, No. 4, 1977, pp. 709–728.

[9] Liu, Y., Kapania, R. K., Gern, F. H., and Inman, D. J., "Equivalent Plate Modeling of Arbitrary Planform Wings," in *Advances in Computational Engineering and Sciences: Proceedings of the International Conference on Computational Engineering and Sciences*, edited by S. N. Atluri and F. W. Brust, 2000, pp. 515–521.

[10] Kapania, R. K., and Liu, Y., "Static and Vibration Analyses of General Wing Structures Using Equivalent-Plate Models," *AIAA Journal*, Vol. 38, No. 7, July 2000, pp. 1269–1277.

[11] Gern, F. H., Inman, D. J., and Kapania, R. K., "Structural and Aeroelastic Modeling of General Planform Wings with Morphing Airfoils," *AIAA Journal*, Vol. 40, No. 4, April 2002, pp. 628–637.

[12] Ramm, E., "Strategies for Tracing the Nonlinear Response near Limit Points," in *Nonlinear Finite Element Analysis in Structural Mechanics*, edited by W. Wunderlich, E. Stein, and K-J. Bathe, Springer–Verlag, Berlin, Heidelberg, New York, 1981, pp. 63–89.

[13] Riks, E., "An Incremental Approach to the Solution of Snapping and Buckling Problem," *International Journal of Solids and Structures*, Vol. 15, No. 7, 1979, pp. 529–551.

[14] Batoz, J. L., and Dhatt, G., "Incremental Displacement Algorithms for Nonlinear Problems," *International Journal for Numerical Methods in Engineering*, Vol. 14, No. 8, 1979, pp. 1262–1267.

[15] Crisfield, M. A., "A Fast Incremental/Iterative Solution Procedure That Handles Snap-Through," *Computers and Structures*, Vol. 13, Nos. 1–3, 1981, pp. 55–62.

[16] Wempner, G. A., "Discrete Approximations Related to Nonlinear Theories of Solids," *International Journal of Solids and Structures*, Vol. 7, No. 11, 1981, pp. 1581–1599.

[17] Bathe, K.-J., "Finite Element Procedures," Prentice–Hall, Englewood Cliffs, NJ, 1996.

[18] Reddy, J. N., "Mechanics of Laminated Composite Plates Theory and Analysis," CRC Press, Inc., Boca Raton, FL, 1997.

[19] Carrera, E., "Comportamento Postcritico di Gusci Multistrato," Tesi di dottorato (Ph.D. Dissertation), Dottorato in Ingegneria Aerospaziale Politecnico di Milano, Politecnico di Torino, Università di Pisa, 1991.

[20] Oñate, E, "On the Derivation and Possibilities of the Secant Stiffness Matrix for Nonlinear Finite Element Analysis," *Computational Mechanics*, Vol. 15, 1995, pp. 572–593

[21] Yamaki, N., "Influence of Large Amplitudes on Flexural Vibrations of Elastic Plates," *Zeitschrift für Angewandte Mathematik und Mechanik*, Vol. 41, 1967, pp. 501–510.

[22] Wang, C. T., "Bending of Rectangular Plates with Large Deflections," NACA, Report No. 1462, 1948.

[23] Levy, S., "Bending of Rectangular Plated with Large Deflections," NACA Report No 737, 1942.

[24] Demasi, L., and Livne, E., "Exploratory Studies of Joined Wing Aeroelasticity," AIAA Paper 2005-2172, 2005.

[25] Levy, R., and Gal, E., "Triangular Shell Element for Large Rotations Analysis," *AIAA Journal*, Vol. 41, 2003, pp. 2505–2508.

[26] Levy, R., and Spillers, W. R., "Analysis of Geometrically Nonlinear Structures," Chapman & Hall, London, 1995.
[27] Attar, P. J., Dowell, E. H., and White, J. R., "Modeling the LCO of a Delta Wing Using a High Fidelity Structural Model," AIAA Paper 2004-1692, 2004.
[28] Dixon, I. R., and Mei, C.,"Finite Element Analysis of Large-Amplitude Panel Flutter of Thin Laminates," *AIAA Journal*, Vol. 31, No. 4, 1993, pp. 701–707.
[29] Gray, C. E., Jr., and Mei, C., "Large Amplitude Finite Element Flutter Analysis of Composite Panels in Hypersonic Flow," *AIAA Journal*, Vol. 31, No. 6, 1993, pp. 1090–1099.
[30] Demasi, L., and Livne, E., "Assessment of the Nonlinear Structural Simple-Polynomial Ritz-Based Equivalent Plate Approach," AIAA Paper 2005-2093, April 2005.